The Slope Imaging Multi-Polarization Photon-Counting Lidar: an Advanced Technology Airborne Laser Altimeter

David Harding[1], Philip Dabney[1], James Abshire[1], Tim Huss[3], Gabriel Jodor[3], Roman Machan[3], Joe Marzouk[3], Kurt Rush[1], Antonios Seas[1], Christopher Shuman[1], Xiaoli Sun[1], Susan Valett[1], Aleksey Vasilyev[2], Anthony Yu[1], and Yunhui Zheng[3]

[1]NASA Goddard Space Flight Center, Greenbelt, MD 20771
[2]Science Systems and Applications, Inc., Lanham, MD, 20706
[3]Sigma Space Corporation, Lanham, MD, 20706

***Abstract* - The Slope Imaging Multi-polarization Photon-counting Lidar (SIMPL) is an airborne instrument developed to demonstrate laser altimetry measurement methods and components that enable efficient, high-resolution, swath mapping of topography and surface properties from space. The instrument was developed through the NASA Earth Science Technology Office Instrument Incubator Program with a focus on cryopshere remote sensing. The SIMPL transmitter is an 11 KHz, 1064 nm, plane-polarized micropulse laser transmitter that is frequency doubled to 532 nm and split into four push-broom beams. The receiver employs single-photon, polarimetric ranging at 532 and 1064 nm using Single Photon Counting Modules in order to achieve simultaneous sampling of surface elevation, slope, roughness and depolarizing scattering properties, the latter used to differentiate surface types. Data acquired over ice-covered Lake Erie in February, 2009 are used to documenting SIMPL's measurement performance and capabilities, demonstrating differentiation of open water and several ice types. The NASA ICESat-2 mission scheduled for launch in 2015 has a focus on monitoring ice sheet elevation change and sea ice thickness. ICESat-2 will employ several of the technologies advanced by SIMPL, including micropulse, single photon ranging in a multi-beam, push-broom configuration operating at 532 nm.**

I. INTRODUCTION

The Slope Imaging Multi-polarization Photon-counting Lidar (SIMPL) is an airborne laser altimeter developed through the NASA Earth Science Technology Office Instrument Incubator Program with a focus on cryosphere remote sensing. The SIMPL instrument incorporates a variety of advanced technologies in order to demonstrate measurement approaches of potential benefit for improved, more efficient airborne laser swath mapping and spaceflight laser altimeter missions. SIMPL incorporates beam splitting of a micropulse laser, single-photon ranging and polarimetry technologies at green (532 nm) and near-infrared (1064 nm) wavelengths. The measurement configuration is a "push-broom" with four beams spaced apart perpendicular to the flight direction (Fig. 1). Operating at both wavelengths and measuring the depolarization of plane-polarized transmit pulses enables differentiation of surface types. The depolarization ratio is sensitive to the proportions of specular reflection and surface and volume scattering, and is a function of wavelength. SIMPL's measurement capabilities provide information about surface elevation, roughness and slope as well as scattering properties intended to differentiate ice sheet and sea ice surface conditions.

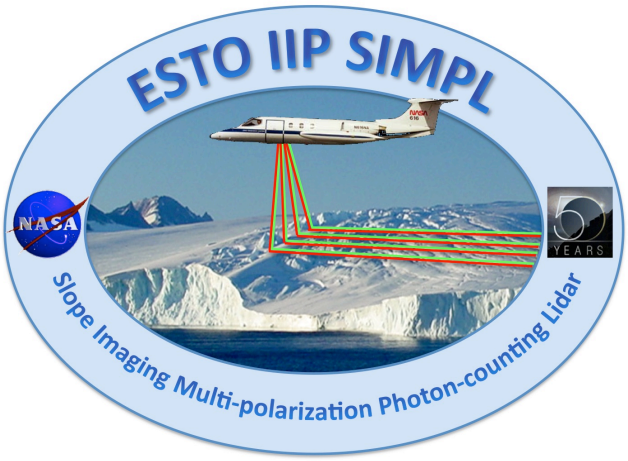

Fig. 1. SIMPL beam geometry with four cross-track, 532 and 1064 nm beams forming four parallel, two-color profiles in the flight direction.

Prior work has demonstrated micropulse, photon-counting laser altimetry at 532 nm using Photomultiplier Tube (PMT) detectors, including the scanning Multikilohertz Photon-Counting Microlaser Altimeter (MMLA) developed in an earlier IIP project [1,2] and the multi-beam Coastal Area Tactical-mapping System (CATS)

[3,4]. In addition earlier work using the Airborne Laser Polarization Sensor (ALPS), a non-range resolved instrument, documented that laser depolarization at 355, 532 and 1064 nm differentiates needle-leaf and broad-leaf vegetation, as well as a variety of row crops, based on differences in their wavelength-dependent scattering properties [5,6]. The Multi-wavelength Polarimetric Airborne Lidar (MAPL) is a modification of ALPS incorporating full waveform recording, enabling polarimetric ranging at 532 and 1064 nm [7,8]. Range-resolved, horizontal-path ground measurements using MAPL also showed differentiation of tree species. SIMPL integrates and advances these technologies in a 16-channel instrument having four beams each with two colors, with each color observed in directions parallel and perpendicular to the transmit polarization plane.

II. INSTRUMENTATION

A. *Transmitter*

SIMPL's laser transmitter and receiver optics are mounted on opposite sides of a thermally stable, 80 cm long optical bench and share the same 20 cm aperture off-axis parabola telescope in order to preserve alignment between the transmitter and receiver (Fig. 2). The micropulse transmitter source is an 11.4 kHz pulse rate, 1064 nm (near infrared) microchip laser manufactured by Teem Photonics that emits ~8 microjoules per pulse of linearly polarized light. The pulse width is approximately 1 nsec (full-width at half the peak amplitude, FWHM) equivalent to 15 cm. The NIR output is frequency doubled to 532 nm (green) using a KTP nonlinear crystal. The dual wavelength beam is then spectrally separated using a dichroic beam splitter and each color goes through its own transmit optical path. Each optical path separates the beams into four beams with parallel polarization planes. The two wavelength beam paths are then recombined using a dichroic filter such that the two colors on each of the four beams are co-aligned. A lens array is used to provide a specified beam divergence and angular spread of the four beams when transmitted toward the Earth's surface through the telescope. The result is four 0.3 m laser footprints with each spaced cross-track by 8 m at the nominal flight altitude of 3.7 km (12,000 ft).

B. *Receiver*

Laser energy reflected from the Earth's surface is collected by the primary mirror and is directed into the receiver using turning mirrors. A lens assembly focuses the received beams onto a pinhole plate that has a 1 x 4 pinhole array. The pinholes define the detector fields of view (FOV) that are 0.9 m at the nominal flight altitude. The FOVs are small, only three times the size of the transmit beam divergence, to provide strong spatial filtering of solar background radiation.

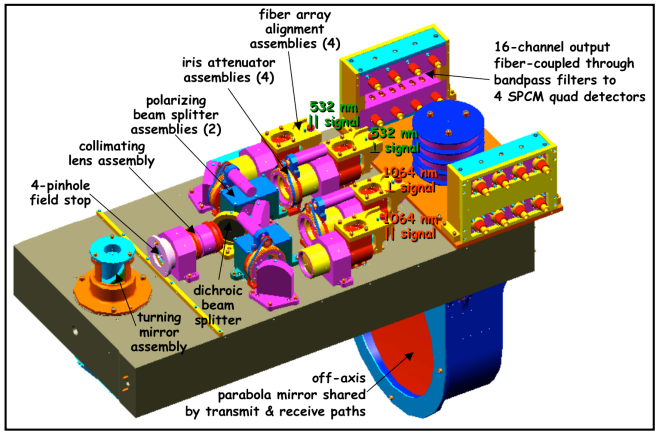

Fig. 2. Mechanical schematic of the SIMPL optical bench and receiver-side components.

The 532 and 1064 nm beams are then separated by a dichroic plate and each wavelength is further decomposed into signals with polarization parallel and perpendicular to the transmit polarization plane. The end result is four beam arrays that each have a particular wavelength and polarization state, yielding 16 signal channels. Each beam array passes through a mechanical iris used to control the effective receiver aperture and thus control signal and solar background count rates.

Using fibers the 16 channels are passed through spectral filter assemblies to further reduce the solar background noise. Fibers are then used to transfer the filtered light to 16 Single Photon Counting Modules (SPCMs) manufactured by PerkinElmer. SPCMs are silicon avalanche photodiodes (Si:APD) that emit an electrical pulse upon detection of a single photon [9]. SPCM's are used because they are the only mature, single photon, time-resolved detectors with sensitivity at both 532 nm and 1064 nm. Their 532 nm quantum efficiency (QE) is between 60 to 70% whereas the 1064 nm QE is very low, at about 2%. A disadvantage of the SPCM's is that after detection of a photon they have a dead time of ~ 50 nsec (7.5 m) during which additional received photons cannot be detected. The dead time causes a range that is too short if one or more signal photons per laser pulse are received within 50 nsec of the first detected photon. To avoid a range bias the probability of detecting a signal photon per laser fire on each channel is controlled, using the mechanical irises and by changes in flight altitude, to nominally be below 30% so that the probability of two signal photons being received within 50 nsec is small.

C. *Electronics*

Upon detection of a photon, the electrical pulse from an SPCM is transmitted to one of four custom electronics interface cards. Each card receives signals from a four-beam array, consisting of signals for a wavelength and polarization state. In addition a signal for each laser fire time and a GPS once-per-second pulse are distributed to each card. In each card the signals from four detectors, start pulse and GPS time tick are temporally offset, combined together and uniquely tagged. The combined events are transmitted to one of four P7889 event timer cards manufactured by FAST ComTec that are housed in the flight computer. The cards time tag each event with 100 psec resolution. The high precision timing and short laser pulse width achieve a single photon range precision of ~7 cm.

D. *Data System*

A sustained data rate up to 22 million time-tagged events per second recorded to RAID disk storage has been achieved by the data system. Photon detection events are not range gated; following a laser fire detection events are recorded for all ranges from just outside the aircraft to a distance of 13 km. In this way, atmospheric profiling can be done to characterize cloud cover conditions through which the ranging measurements are made. The 22 million events per second data rate accommodates the maximum expected solar background noise counts acquired from throughout the 13 km range window assuming a high solar inclination angle, a highly reflective surface such as snow and fully open irises. Because detection events from throughout the 13 km window are recorded noise counts dominate the detection events; typically only a few percent or less of the events are returns reflected from the surface. Post-flight processing software unpacks the data and sorts it by laser wavelength and polarization and computes the UTC event time and time-of-flight for each detected photon.

Ancillary instrumentation consists of an Applanix Pos-AV system that provides orientation, position and time information and a nadir-viewing, digital video camera with latitude, longitude and time labeling to document the flight line. The SIMPL flights have been conducted on the NASA Lear-25 aircraft operated by Glenn Research Center. The Lear-25 has a nadir viewing, optical port over which the optical bench is installed in a mounting frame. The additional SIMPL instrumentation is installed in two half-height 19-inch flight racks, including the fiber-coupled SPCM detectors, power supplies, power meter, laser and temperature controllers, video equipment, receiver electronics, flight computer and RAID storage.

III. MEASUREMENT CHARACTERISTICS

The fundamental character of the SIMPL data is a "point cloud" profile of single photon ranges including spatially correlated surface returns and randomly distributed solar background noise (Fig. 4). Aggregation of returns from a surface yields a range histogram that is a function of the transmit pulse shape, laser fire timing jitter, receiver bandwidth, surface "slope" (the incident angle between the laser beam and the surface normal), surface roughness at the laser footprint scale, and penetration into the surface and resulting volume scattering if the material is partly transparent at the laser wavelength. The SIMPL transmit pulse shape consists of two components, a main pulse, that is slightly asymmetric and positively skewed, and a broader, weaker after-pulse that occurs 8.3 nsec (1.25 m) after the main pulse. At 1064 nm the amplitude of the after-pulse is 20% of the main pulse. Frequency doubling to 532 nm reduces the amplitude of the after-pulse to 6% of the main pulse. The instrument impulse response, established by laboratory measurements of the return from a smooth, non-transparent surface perpendicular to the laser beam, accounts for the transmit pulse, timing jitter and receiver bandwidth. For SIMPL the impulse response of the main pulse is 1 nsec FWHM, equivalent to 15 cm. Broadening of the range histogram main pulse beyond 1 nsec is due to the combined effects of surface slope, roughness and penetration.

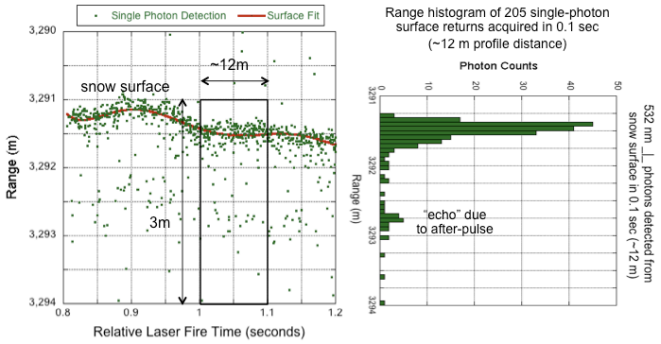

Fig. 4. SIMPL single photon point cloud (532 nm perpendicular polarization) from a smooth, undulating snow surface (left) and an 18 cm FWHM range histogram for 205 photons reflected from a flat segment acquired in 0.1 sec (right), corresponding to 12 m at the nominal aircraft ground speed.

The amplitude of the range histogram depends on the probability of detection (PD), defined as the ratio of received photons reflected from the surface versus the number of transmitted pulses. The PD is a function of the surface retro-reflectance (at 0° phase angle with parallel illumination and view angles), ranging distance, atmospheric transmission and instrument parameters including transmit energy, telescope aperture, iris

vignetting, beam to pinhole alignment, receiver optical throughput and detector sensitivity. At the 11.4 kHz pulse rate and nominal aircraft ground speed, flight altitude and iris aperture settings, single photons are typically acquired from ice surfaces every 3, 4, 6 and 9 cm for the 532 nm parallel (||) and perpendicular (_|_) channels and the 1064 nm || and _|_ channels, respectively.

III. ICE-COVERED LAKE ERIE RESULTS

SIMPL acquired data over Lake Erie on February 25, 2009 when ice cover was extensive (Fig. 3). Great Lake ice cover during the winter of 2008-2009 was the fourth greatest since 1986-1987 [10]. The ice cover, analogous to young sea ice, was a heterogeneous amalgam of fresh skim ice, thin dark and light nilas ice, and fractured areas of new grey ice and thicker new grey-white ice. There are extensive areas of breccia consisting of ice pieces of different types and sizes frozen together. The lake ice is covered by snow in some places and broken by open water leads and polynya (non-linear shaped openings enclosed in ice).

Fig. 3. Oblique aerial photograph of Lake Erie Ice cover form the NASA Lear-25 on February 25, 2009.

Measurement results for Lake Erie are illustrated here using a ~260 m long flight segment crossing an open water lead, a polynya covered by skim ice, dark nilas ice and new grey-white ice (Figs. 5, 6 and 9). The character of the point cloud differs for the four channels illustrated by Beam 3 in Fig. 5. The PD is indicated by the density and thickness of the surface return point cloud. The strength of the after-pulse relative to the main pulse is reduced at 532 nm due to frequency doubling. Solar background noise is substantially larger at 532 nm due to higher solar irradiance and, for snow and ice surfaces, higher reflectance at that wavelength as compared to 1064 nm.

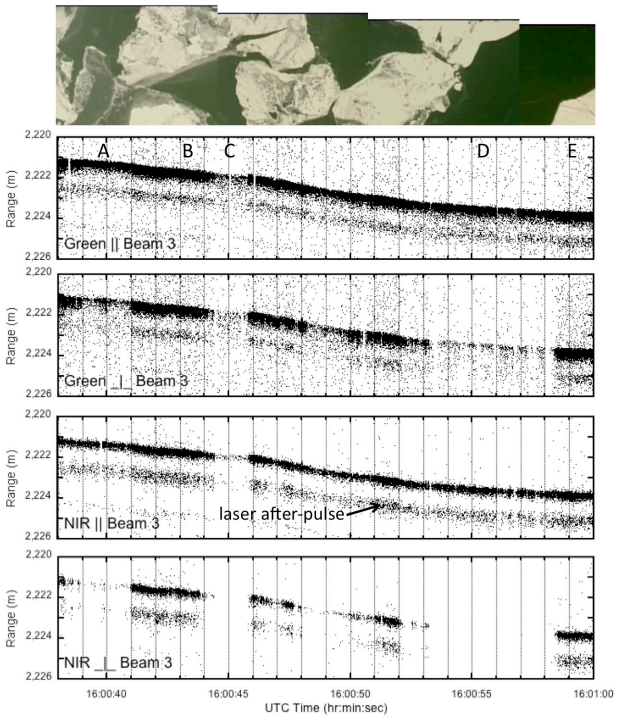

Fig. 5. Point cloud profiles across Lake Erie ice cover for the four channels on Beam 3. From top to bottom they are the 532 nm parallel and perpendicular channels and the 1064 nm parallel and perpendicular channels. The profile location is along the bottom edge of the video frame composite. Based on interpretation of the video, four surface types occur along the profile: dark nilas ice (A), new grey-white ice (B, E), polynya covered by skim ice (C) and an open water lead (D). The profile length is ~ 260 m. The surface slope is due to uncompensated aircraft roll. The surface echo is due to the laser after-pulse. The vertical exaggeration is 43x.

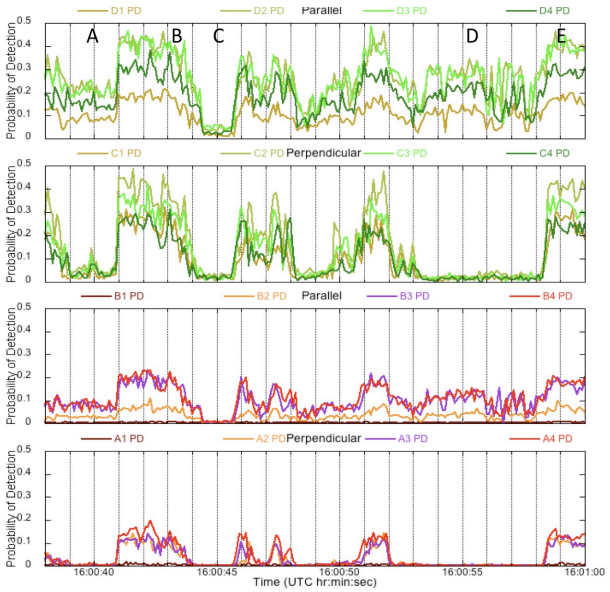

Fig. 6. Probability of detection for beams 1, 2, 3 and 4 on each channel. The channel order is the same as that of Fig. 5. No 1064 nm || nor _|_ signal is detected for Beam 1 due to very low transmit energy, documented by lab per-beam power measurements, and beam to pin-hole misalignment observed while optically aligning the instrument.

Fig. 6 shows the PDs for the same flight segment, computed for one-second increments, for the four channels along the four beams. Significant variability is observed between the channels and along the profiles. Between-beam consistency at short length scales for each channel indicates that the variability is not noise. Amplitude differences between a channel's four beams are due to instrumental effects. Changes in PD are correlated with surface types having different reflectance and scattering properties. For single scatter events the reflecting photon's polarization plane remains parallel to that of the transmit pulse. In the case of specular reflection from a mirror-like surface or from water, consisting only of single scattering, all reflected energy retains a parallel polarization plane. This accounts for the lack of 1064 nm _|_ signal from open water (D). The strength of the 532 and 1064 nm || signal specularly reflected back to the receiver depends on the fraction of the water surface that is oriented perpendicular to the incident beam. That depends on the water surface roughness, primarily a function of wind speed [11].

During multiple scattering from non-specular surfaces and from volume scattering in semi-transparent materials, the polarization plane of some reflected photons are rotated to be perpendicular to that of the incoming laser pulse. The weak 532 nm _|_ signal is due to volume scattering of green light that penetrated into the water column. The strength of the water column return is a function of the waters optical depth. An equivalent amount of 1064 nm light penetrates into the water column but it is all absorbed over a distance of a few cms due to water's high near-infrared absorption coefficient. The new grey-white ice (B, E) yields substantial signals in all four channels indicating that multiple scattering from a diffusely reflecting surface is occurring. The signal strengths of the nilas ice (A) are intermediate between that of the open water and the new grey-white ice suggesting that a combination of specular, diffuse and volume scattering is occurring.

The polynya with skim ice cover has no 1064 nm _|_ signal, very weak || signal and low 532 nm || and _|_ signals. It is inferred that the smooth skim ice is specular and, unlike the wind-roughened water surface, nearly all reflected || laser energy is directed at an angle away from the receiver because the laser beam is not normal to the surface. Micro-roughness is thought to be causing specular reflection of the very weak 1064 nm || signal back to the receiver. The thin skim ice is transparent so green light is penetrating into the water column and undergoing volume scattering, accounting for the low 532 nm signals at both || and _|_ polarizations.

The shapes of the range histograms substantiate this interpretation of the skim ice scattering properties. The histogram shapes for the diffusely scattering new grey-white ice (B) are the same for each of the four channels (Fig. 7). The 1.1 to 1.5 nsec FWHM widths are slightly broadened as compared to the instrument impulse response indicating that the surface is slightly roughened and/or sloped with respect to the incident beam. The shapes for the polynya are substantially different (Fig. 8). The broadened 532 nm || and _|_ signals with skewed tails are water column extinction

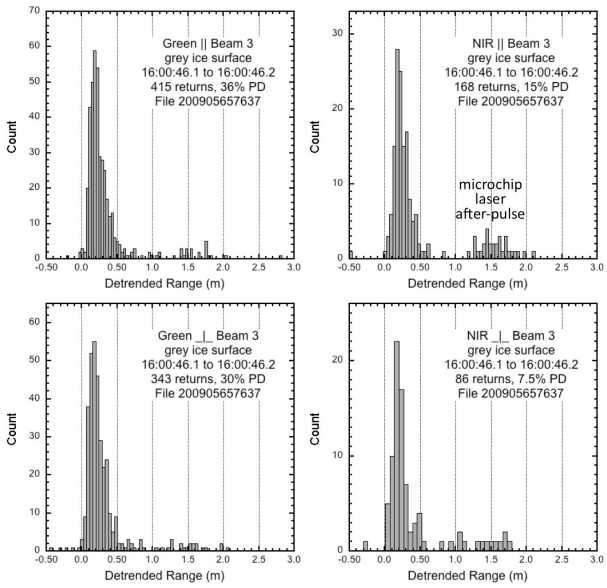

Fig. 7. New white-grey ice (B) single photon range histograms for the four channels on Beam 3. Y-axis maximum values are adjusted to equalize the peak heights. Number of detected photons in 0.1 sec and the resulting PDs are indicated in the labels for each histogram.

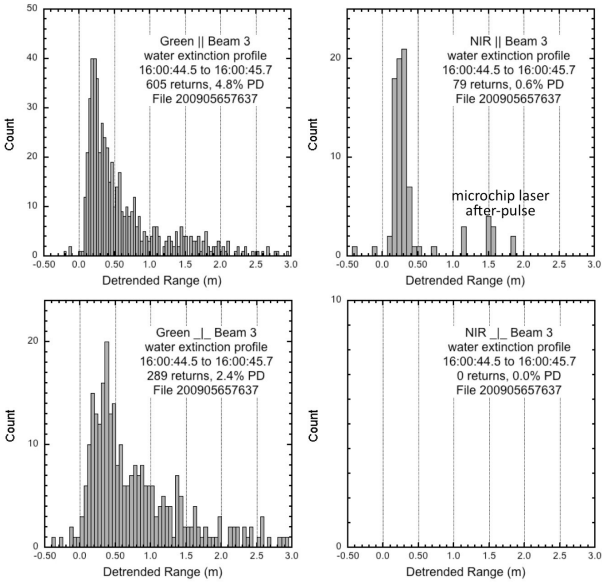

Fig. 8. Skim ice covered polynya (C) single photon range histograms for the four channels on Beam 3. Y-axis maximum values are adjusted to equalize the peak heights. Number of detected photons in 0.2 sec and the resulting very low PDs are indicated in the labels for each histogram.

profiles showing light penetration to a depth of 3 m. With increasing depth the _|_ signal becomes more dominant as compared to the || signal due to greater multiple scattering further in the water column. The very weak, narrow 1064 nm || signal is consistent with minor a specular return from the water surface. No 1064 nm _|_ signal is detected because the surface return is specular (only ||) and high near-surface absorption in the water column eliminates volume scattering.

The changes in PD for the different surface conditions result in distinctive depolarization ratios, computed as the ratio _|_ PD / || PD. A completely specular return has a depolarization ratio of 0. With increasing multiple scattering, the depolarization ratio increases. Fig. 9 shows depolarization ratios for the same flight segment depicted in Figs. 5 and 6. The ratios are normalized by the depolarization of a snow calibration surface, so that a surface with a value of 1 has depolarization equivalent to that of the snow target. Values greater than 1 are due to scattering causing depolarization greater than that of snow. The equivalent ratios, per wavelength, for each of the beams spaced cross-track by ~8 m indicates that they are traversing surfaces with the same scattering properties, except for a short segment occurring at 16:00:50. The open water (D) has very low and near-zero 532 and 1064 nm ratios, respectively. The nilas ice (A) ratios are similar except for a higher ratio corresponding to a lighter ridge observed in the video frame. The new white-grey ice (B, E) has ratios comparable to that of the snow calibration target. The polynya with the skim ice cover has noisy ratios due to the very low || signals at both 532 and 1064 nm.

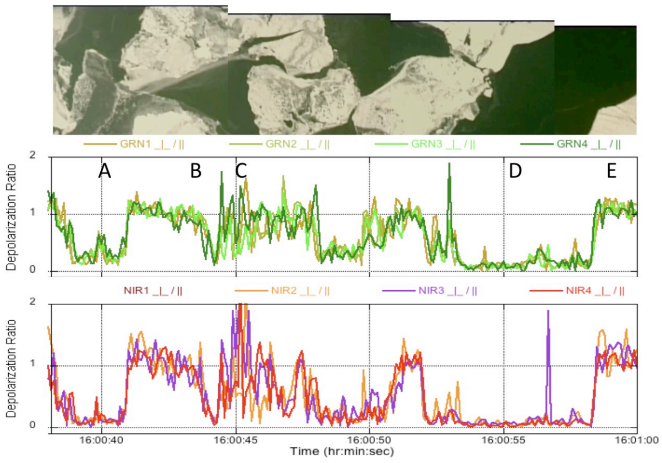

Fig. 9. 532 and 1064 nm _|_ / || depolarization ratios for the four beams along the same flight segment depicted in Figs. 5 and 6. There is no 1064 nm ratio for Beam 1 due to the absence of _|_ and || signals.

IV. SIMPL AND THE ICESAT-2 MISSION

The experience gained concerning micropulse, single-photon ranging of cryosphere surfaces using SIMPL is benefiting formulation activities for the ICESat-2 mission. ICESat-2 will be a follow-on to NASA's Ice, Cloud and land Elevation Satellite (ICESat) that operated between 2003 and 2009. ICESat had a primary measurement goal of ice sheet elevation change and secondary goals for land topography, forest canopy height and atmosphere cloud and aerosol profiling [12,13]. During the course of the mission measurement of sea ice thickness and its change became an additional area of primary focus [14,15]. Its single instrument, the Geoscience Laser Altimeter System (GLAS) [16], utilized a single-beam, 40 Hz, high pulse energy laser transmitter and the receiver combined a 1064 nm laser altimeter with 3 cm ranging precision and a 1064 and 532 nm cloud and aerosol lidar that profiled the atmosphere with 75 m vertical sampling. The analog 1064 nm channels acquired ranging data using the traditional measurement approach, waveform digitization of strong return pulses, whereas the 532 nm lidar channel utilized single photon ranging with SPCM detectors.

The ICESat-2 follow-on [17], scheduled for launch in 2015, has the same objectives as ICESat but will employ the measurement approach used by SIMPL. It will utilize a micropulse laser with a narrow pulse width (several nsec) operating at a high pulse repetition rate (10 to 15 kHz). The low transmit pulse energy will be divided into a multiple beam, push-broom configuration (Fig. 10). The receiver will conduct all ranging using time-tagged single photon detection at 532 nm, currently planning use of PMT array detectors, with 100 psec timing resolution electronics. (At

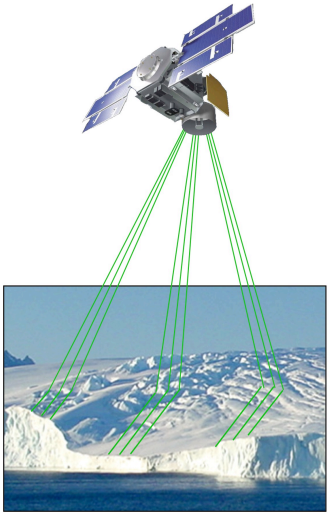

Fig. 10. Current concept for ICESat-2's 9 beam configuration (graphic is not to scale).

present there are no plans to simultaneously operate at 1064 nm nor acquire depolarization data.) The concept for the ICESat-2 beam configuration has 9 beams grouped in 3 sets of triplets with 45 m spacing between triplet beams and 3 km spacing between the sets. The triplet beams will be used to measure local surface slope in order to separate slope effects from elevation change measured over time by along-track repeating of the profiles.

SIMPL's data are being used to assess an area of concern for ICESat-2, range-bias effects introduced by 532 nm penetration into snow, ice and water. The data are also being used to assess variability in the probability of detection for these surface types and to develop algorithms for on-board data acquisition and on-ground characterization of surface elevation, slope and roughness. In these ways, the development of the SIMPL instrument is meeting its objective of advancing technologies in order to demonstrate measurement approaches of benefit for improved, more efficient spaceflight laser altimeter missions.

REFERENCES

[1] J.J. Degnan, J. McGarry, T. Zagwodzki, P. Dabney, J. Geiger, R. Chabot, C. Steggerda, J. Marzouk and A. Chu, "Design and performance of an airborne multikilohertz photon-counting, microlaser altimeter," *Proc. Land Surface Mapping and Characterization using Laser Altimetry, Int. Arch. Photogramm. Rem. Sens.*, vol. XXXIV3-W4, Annapolis, MD, pp. 9-16, 2001.

[2] J.J. Degnan, "Photon-counting multikilohertz microlaser altimeters for airborne and spaceborne topographic measurements," *J. Geodyn*., vol. 34(3-4), pp. 503-549, 2002.

[3] W.E. Carter, R.L. Shrestha and K.C. Slatton, "Photon counting airborne laser swath mapping (PC-ALSM)," in Gravity, Geoid and Space Missions, C. Jekeli, L. Bastos and J. Fernandes (Eds), Springer, IAG International Association of Geodesy Symposia, Vol. 129, pp. 214 - 217, 2004.

[4] T. Cossio, C. Slatton, W. Carter, K. Shrestha and D. Harding, "Predicting topographic and bathymetric measurement performance for low-SNR airborne lidar," *IEEE Trans. Geosci. Rem. Sens.*, vol. 47(7), pp. 2298 – 2315, 2009.

[5] J. E. Kalshoven, Jr., and P. W. Dabney, "Remote sensing of the Earth's surface using an airborne polarized laser," *IEEE Trans. Geosci. Remote Sensing*, vol. 31, pp. 438–446, 1993.

[6] J.E. Kalshoven, Jr., M.R. Tierney, Jr., C.S. T. Daughtry and J.E. McMurtrey III, "Remote sensing of crop parameters with a polarized, frequency-doubled Nd:YAG laser," *Appl. Opt.*, vol. 34, pp. 2745-2749, 1995.

[7] S. Tan, and R. Narayanan, "Design and performance of a multiwavelength airborne polarimetric lidar (MAPL) for vegetation remote sensing," *Appl. Opt.*, vol. 43(11), pp. 2360-2368, 2004.

[8] S. Tan, R.M. Narayanan, and S.K. Shetty, "Polarized Lidar Reflectance Measurements of Vegetation at Near-Infrared and Green Wavelengths," *Int. J. Infrared Millimeter Waves,* Vol. 26(8), pp. 1175-1194, 2005.

[9] X. Sun, M.A. Krainak, J.B. Abshire, J.D. Spinhirne, C. Trottier, M. Murray, H. Dautet, G.R. Allan, A.T. Lukemire, J.C. Vandiver, "Space-qualified silicon avalanche-photodiode single-photon-counting modules," *J. Modern Optics,* vol. 51(9), pp.1333-1350, 2004.

[10] J. Wang, X. Bai, G.A. Leshkevich, M.C. Colton, A.H. Clites, and B.M. Lofgren, "Severe ice cover on Great Lakes during winter 2008-2009," *EOS Trans.*", vol. 91(5), pp. 41-42, 2010.

[11] J.L. Bufton, F.E. Hoge and R.N. Swift, "Airborne measurements of laser backscatter from the ocean surface," *Appl. Opt.*, vol. 22, pp. 2603-2618, 1983.

[12] H.J. Zwally, R. Schutz, W. Abdalati, J. Abshire, C. Bentley, J. Bufton, D. Harding, T. Herring, B. Minster, J. Spinhirne and R. Thomas, "ICESat's laser measurements of polar ice, atmosphere, ocean, and land", *J. Geodyn*., vol. 34(3-4), pp. 405-445, 2002.

[13] B.E. Schutz, H.J. Zwally, C.A. Shuman, D. Hancock, J.P. DiMarzio, "Overview of the ICESat Mission," *Geophys. Res. Lett.*, vol. 32: L21S01, doi:10.1029/2005GL024009, 2005.

[14] R. Kwok, H.J. Zwally and D. Yi, "ICESat observations of Arctic sea ice: A first look," *Geophys. Res. Lett*., vol. 31:L16401, doi: 10.1029/2004GL020309, 2004.

[15] R. Kwok, G. F. Cunningham, M. Wensnahan, I. Rigor, H. J. Zwally, and D. Yi, "Thinning and volume loss of the Arctic Ocean sea ice cover: 2003–2008," *J. Geophys. Res.*, vol. 114: C07005, doi:10.1029/2009JC005312, 2009.

[16] J. Abshire, X. Sun, H. Riris, M. Sirota, J. McGarry, S. Palm, D. Yi and P. Liiva, "ICESat: GLAS on orbit science measurements through March," *Geophys. Res. Lett.*, vol. 32: L21S01, doi:10.1029/2005GL024028, 2005.

[17] W. Abdalati, et al., "The ICESat-2 Laser Altimetry Mission," *Proc. IEEE*, vol. 98(5), pp. 735-751, 2010.